Available online at www.sciencedirect.com
ScienceDirect
Materials Research Bulletin 43 (2008) 3562–3569
Materials Research Bulletin
www.elsevier.com/locate/matresbu

Formation of hollow NiO single crystals and Ag/NiO flowers

Fei Teng [a,b,*], Tongguang Xu [b], Youfei Zheng [a], Shuhui Liang [b], Bulgen Gochoo [b], Xiaohua Gu [b], Ruilong Zong [b], Wenqing Yao [b], Yongfa Zhu [b,*]

[a] College of Environmental Science and Technology, Nanjing University of Information Science & Technology, Nanjing 210044, PR China
[b] Department of Chemistry, Tsinghua University, Beijing 100084, PR China

Received 29 November 2006; received in revised form 13 December 2007; accepted 14 January 2008
Available online 20 January 2008

Abstract

In this work, the $Ni(OH)_2$ core–shell nanostructures were fabricated by a hydrothermal method without using any templates. After the core–shell sample was annealed, the novel hollow NiO nanostructures were obtained. The Ostwald ripening process was proposed to elucidate the formation of the samples. Moreover, Ag/NiO flowers were prepared by impregnating hollow NiO particles with $Ag(NO_3)_3$ solution. The samples were characterized by TEM, HREM, SAED, XRD, BET, SEM and EDS methods. Most importantly, Ag/NiO flowers and hollow NiO nanostructures exhibited the excellent catalytic activities for CO oxidation.

Keywords: A. Nanostructures; B. Chemical synthesis; C. Crystal growth; D. Catalytic properties

1. Introduction

Hollow micro- and nano-structures, as a new class of materials, have unique physicochemistry properties different from those of their solid counterparts, including light weight, high surface area and good permeation. Therefore, they are increasely demanded in a variety of new technological applications, such as artificial cells, catalysts, fillers, coatings, pigments, drugs delivery and dyes [1–5]. A variety of hollow structures, including metals, ceramics and inorganic-hetero-composites, have been fabricated [4,6,7]. Generally, the hollow structures are prepared by a template method, including ''hard templates'' (e.g. polymeric beads) [1,3,4,8–12] and ''soft templates'' (e.g. emulsion dropes) [3,13–16]. However, the polymers or surfactants are generally used for the template methods, which have to be removed to create the hollow interior; the template method is time-consuming [10] and expensive; and the obtained materials are usually unstable. Therefore, the practical applications of template route are limited. Recently, the hollow metal oxides have been prepared using Ostwald ripening, in which a direct solid evacuation has occured [17–27]. Liu and Zeng [27] have prepared the hierarchic structures through Ostwald ripening, and the synthesized microspheres have a high thermal stability and a high surface area. The template-free synthesis of hollow structures is an attractive method.

$Ni(OH)_2$ crystals have attracted much attention as an import electrode material in rechargeable batteries [28]. Nevertheless, its electrochemical performance is unsatisfactory for high-rate and high-temperature charge/discharge

* Corresponding authors. Tel.: +86 25 5873 1090; fax: +86 10 6278 7601.
E-mail addresses: tfwd@163.com (F. Teng), zhuyf@mail.tsinghua.edu.cn (Y.F. Zhu).

0025-5408/$ – see front matter © 2008 Elsevier Ltd. All rights reserved.
doi:10.1016/j.materresbull.2008.01.009

applications due to the inactiveness of the material in the core region [29]. Hollow $Ni(OH)_2$ spheres have been synthesized using poly(styrenemethyl acrylic acid) (PSA) particles as templates. However, the as-prepared hollow sample is poorly crystallized and is lack of structure stability. Recently, Wang et al. [30] have prepared hollow $Ni(OH)_2$ and NiO microspheres without using any templates; and the β-$Ni(OH)_2$ crystals were completely converted into the hollow NiO crystals after being annealed at 600 °C for 2 h [31]. NiO is a very prosperous material used in various fields, such as catalysis [32], battery cathodes [33], fuel cell electrodes [34]. To the best of our knowledge, however, the studies on hollow NiO nanostructures with thermal stability are scarely reported [10,35–39]. It is still a big challenge to fabricate hollow materials with a high crystallinity and stability.

In this work, a simple hydrothermal approach was exploited to fabricate the $Ni(OH)_2$ core–shell particles; and the novel hollow NiO single crystals were obtained by annealment. Further, Ag/NiO flowers were obtained by an impregnation method. The samples were characterized by TEM, HREM, SAED, SEM, EDS, XRD and N_2 adsorption. Their catalytic activities for CO oxidation were also evaluated.

2. Experimental

2.1. Sample preparation

In this experiment, all the chemicals, $NiCl_2{\cdot}6H_2O$ (A.R.) and KOH (A.R.), were purchased from Beijing Chemicals Company in China and used without further purification. The hydrothermal synthesis of $Ni(OH)_2$ core–shell particles was carried out at 200 °C for 24 h. Typically, 3.8 g of $NiCl_2{\cdot}6H_2O$ was dissolved in 20 ml of deionized water; then 1.6 M KOH solution was added to the above solution under ultrasonic condition. The pH value of the mixture was adjusted to 9. After sonication for 20 min, the mixture was poured into a Teflon-autoclave (50 ml) and deionized water was supplemented to make 80 vol.% loading. The autoclave was heated at 200 °C for 24 h. After cooling to room temperature naturally, the solids were separated by centrifuging, washed with deionized water, and then completely dried at 80 °C overnight in an oven. To obtain the hollow NiO particles, the core–shell sample was annealed in air. The temperature was ramped to 200, 350–550 °C at a rate of 0.5 °C min^{-1} and was kept at these temperatures for 3 h, respectively. To obtain the nanoplates, the hydrothermal reaction was carried out at 80 °C for 24 h, and all other procedures were same as the above.

To obtain the Ag/NiO flowers, 2 g of hollow NiO particles were dispersed into 20 ml solution of 0.5 M $Ag(NO_3)_3$ under ultrasonic condition. After sonication for 30 min, the sample was subjected to irradiation for 5 h under ultra-red lamp.

2.2. Characterization

The samples were characterized by X-ray diffraction (XRD) on a Rigaku D/MAX-RB X-ray powder diffractometer, using graphite monochromatized Cu Kα radiation (λ = 0.154 nm), operating at 40 kV and 50 mA. The patterns were scanned from 10° to 70° (2θ) at a scanning rate of 5° min^{-1}. A nitrogen adsorption isotherm was performed at 77 K on a Micromeritics ASAP2010 gas adsorption analyzer. Before the measurement, the catalyst was degassed at 200 °C for 5 h. Surface areas of the catalysts were calculated by the BET (Brunauer–Emmett–Teller) method. The morphology of the catalyst was characterized by transmission electron microscopy (TEM, JEOL 200CX) with the accelerating voltage of 200 kV. High-resolution transmission electron microscopy (HRTEM, JEOL JEM-2010) was used to determine the structure of the catalyst. The powder was dispersed in ethanol ultrasonically, and then a drop of liquid was deposited on a thin amorphous carbon film supported by the copper grids. The morphology and compositions of the sample were also characterized by SEM (KYKY 2800) equipped with a Link ISIS EDS analyzer. The acceleration voltage was 15 keV and the current was 1.2 nA. In the recording of X-ray map, a current of 6.7 nA was used.

2.3. Evaluation of activity for CO oxidation

The oxidation reaction of CO was carried out in a conventional flow system under atmospheric pressure. 0.1 g of catalyst was loaded in a quartz reactor (inner diameter: 5 mm), with quartz beads packed at both ends of the catalyst bed. The thermal couple was placed in the catalyst bed to monitor the reaction temperature since CO oxidation is an

exothermic reaction. Before each run, the catalyst was flushed with air (100 ml min^{-1}) at 500 °C for 1 h in order to remove adsorbed species from the surface, and then cooled to 30 °C. A mixture gas of 2 vol.% CO and 98 vol.% air was fed into the catalyst bed at a gas hourly space velocity (GHSV) of 12,000 h^{-1}. The inlet and outlet gas compositions were analyzed by an on-line gas chromatography with a GDX-403 GC-column (1.5 m × 4 mm, 100 °C) and a flame ionization detector (FID).

3. Results and discussion

3.1. Morphologies and crystal structures of the samples

Fig. 1a shows the micrographs of the $Ni(OH)_2$ particles synthesized at 200 °C for 24 h. The sizes of these particles are about 100–150 nm. A clair-obscure contrast between the inner and outer regions of the particle can be observed, indicating the formation of core–shell structure. Interestingly, the core does not locate in the center region, but in the fringe region. In Fig. 1(c and d), the SAED patterns of both core and shell can be indexed to the hexagonal β-$Ni(OH)_2$. This confirms that the core and shell have the same crystal structures. In Fig. 1d, some faint diffraction spots, which resulted from the crystals in shell, can be observed around the bright diffraction spot. This may indicate the separation of shell and core. Fig. S1 (See supporting information) shows the TEM images containing tens of particles and HRTEM images of an individual $Ni(OH)_2$ particle. The lattice spacing could be observed clearly, which confirms the single crystalline properties of the core–shell. The calculated interplanar spacings are 0.27 nm, which correspond to the (0 1 0) planes. It seems that the $Ni(OH)_2$ crystals preferentially grew along the (0 1 0) planes. In order to investigate the effect of temperature on the morphology and structure of the particles, the hydrothermal synthesis was also carried out at 80 °C for 24 h. Observed from Fig. 1b, only irregular $Ni(OH)_2$ nanoplates were obtained, which had 50–100 nm in sizes. It seems that a higher hydrothermal temperature favors for the formation of the core–shell structures, but a lower temperature does not.

A suitable anealing way was employed to control the structure of NiO samples. Fig. 2 gives the TEM micrographs of the samples after anealment. It can be observed that after being annealed, most of the cores have ''hollowed out'' and the hollow NiO nanostructures formed. The sizes of hollow NiO particles are ca. 100 nm and the sizes of hollow interiors are 10–20 nm. It is obvious that the sizes of the hollow NiO particles are smaller than those of their precursor ($Ni(OH)_2$), which may be due to the thermal condensation. Contrastively, the NiO nanoplates of 100 nm in size were obtained by annealing the $Ni(OH)_2$ nanoplates under the same conditions (Fig. 2b). HRTEM was performed to reveal crystal structure of hollow NiO sample (in Fig. 3). The interplanar spacing is 0.24 nm, which corresponds to the (1 1 1) plane of a cubic NiO crystal. This indicates that the hollow NiO crystals preferentially grew along the (1 1 1) planes. The selected area ED patterns confirmed that the hollow NiO has a cubic structure with a lattice parameter of $a = 0.41780$ nm. Moreover, ED patterns on the whole area of an isolated hollow particle are shown in Fig. S2 (See supporting information). The electron diffraction patterns also confirm the single crystalline properties of hollow NiO. Further, the $Ni(OH)_2$ core–shell and hollow NiO particles were also characterized using SEM and EDS. We can

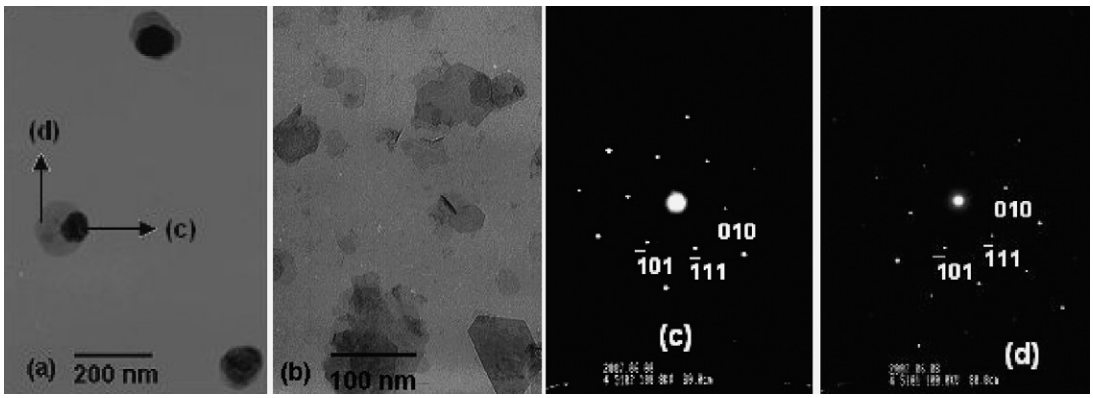

Fig. 1. TEM images and SAED patterns of $Ni(OH)_2$ samples prepared at different hydrothermal temperatures: (a) the $Ni(OH)_2$ core–shell particles prepared at 200 °C, for 24 h; (b) the Ni $(OH)_2$ nanoplates prepared at 80 °C for 24 h; (c) the core of sample (a) and (d) the shell of sample (a).

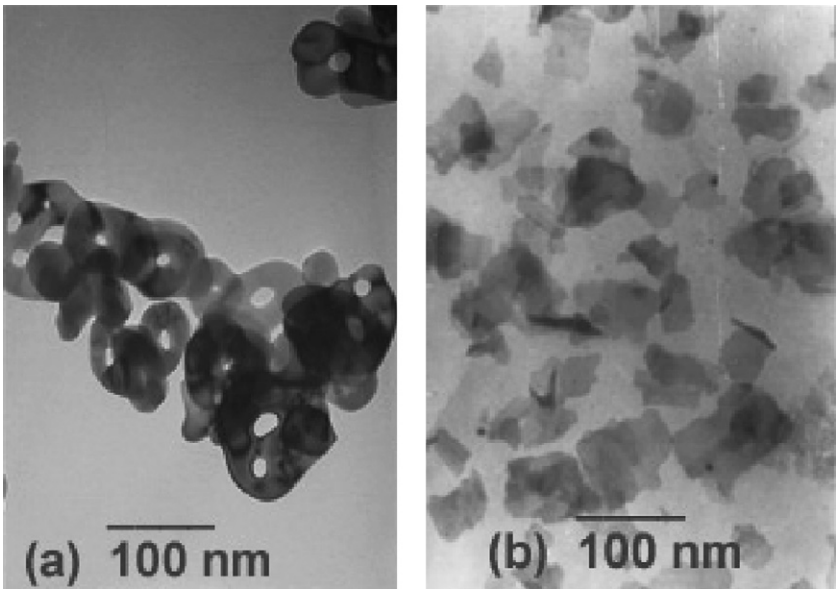

Fig. 2. TEM images of the NiO samples prepared from the annealed $Ni(OH)_2$ samples at 550 °C for 3 h: (a) hollow NiO and (b) plate-like NiO.

observe that both $Ni(OH)_2$ and NiO particles are uniform, as shown in Figs. S3 and S4 (See supporting information). Fig. 4 gives the XRD patterns of the $Ni(OH)_2$ and NiO samples. In Fig. 4(a and b), the as-prepared $Ni(OH)_2$ samples can be both identified as the single-phase β-$Ni(OH)_2$ crystals with a hexagonal structure ($a = 0.3126$ nm, $c = 0.4605$ nm, JCPDS file No. 14-0117). In Fig. 4(c and d), all the diffraction peaks of both NiO samples can be indexed to a face-centered cubic structure (fcc) ($a = 0.41780$ nm, JCPDS file No. 71-1179); no diffraction peaks of β-$Ni(OH)_2$ are observed, indicating that β-$Ni(OH)_2$ crystals have completely converted to NiO crystals. The XRD results are well consistent with the results of SAED analysis (Figs. 1 and 3).

3.2. The proposed formation process of the particles

It has been reported that the structure of particle can be affected by several processes, including crystallization of solids from solution, evolution of gases, intraparticle reactions and interparticle sintering [40]. The growth mechanism of the core–shell structures could be discussed from the results of control experiments. As shown in Fig. S5 (See supporting information), a large number of $Ni(OH)_2$ nanocrystals formed at 200 °C for 3 h, and they had small sizes

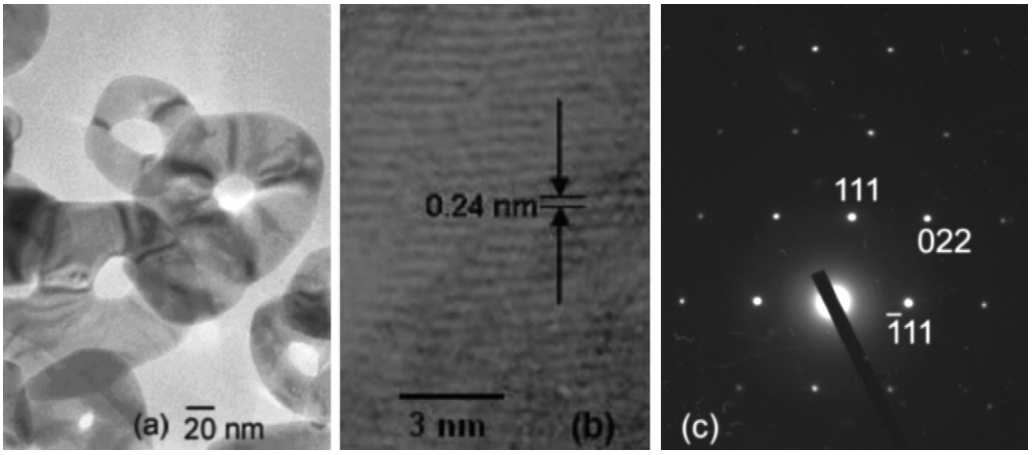

Fig. 3. HRTEM images and SAED patterns of the hollow NiO sample: (a) HRTEM images; (b) Lattice images and (c) SAED patterns.

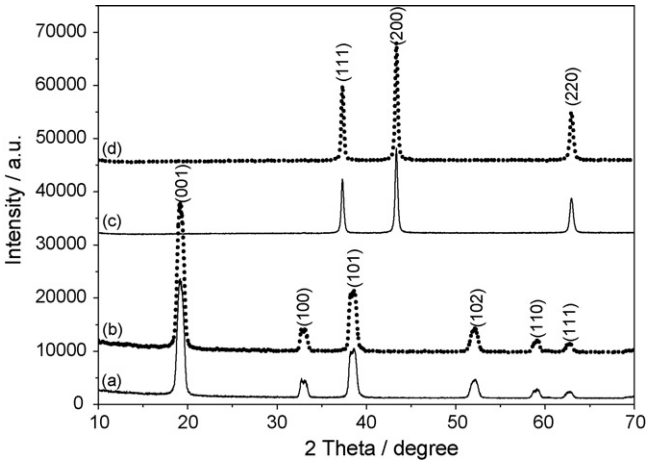

Fig. 4. XRD patterns of $Ni(OH)_2$ and NiO samples: (a) the core–shell $Ni(OH)_2$ particles; (b) $Ni(OH)_2$ nanoplates; (c) hollow NiO and (d) NiO nanoplates.

(10–20 nm). XRD patterns confirmed the well crystalline nature of these nanocrystals (Fig. S6 of supporting information). These nanocrystals have aggregated together to form solid aggregates due to their high surface energy. When the hydrothermal treatment was prolonged to 24 h, the $Ni(OH)_2$ core–shell particles formed (Fig. 1a). It could be imagined that Ostwald ripening may have occurred in some of these aggregates. According to the above results, the formation of the core–shell structure can be divided into several steps. First, $Ni(OH)_2$ nanocrystals were formed by the reaction of Ni^{2+} with OH^-. Then, these colloidal $Ni(OH)_2$ nanocrystals would aggregate together due to the high surface energy, within which the mass distribution may differ at different regions owing to the inhomogeneous size and size distribution of crystallites. Since these inhomogeneous crystallites were in a nonequilibrium state (i.e., hydrothermal conditions), and they would further differentiate and redistribute themselves through Ostwald ripening process. In this process, the larger crystallites keep growing while the smaller ones are undergoing mass relocation through dissolving and regrowing [26]. It is reasonable that the larger $Ni(OH)_2$ crystallites, which are located in a certain region within an aggregate, would grow bigger at the expense of smaller crystals through the ''solid-solution-solid'' process. The mass transportation of solids would start from the regions of smaller crystals. Meanwhile, the remained crystallites in these regions would further re-crystallize and form intact shell. In the end, the pristine particle was divided into two discrete parts, i.e., the core–shell structure formed. The formation of hollow structure after being annealed confirmed above expectation.

It is comprehensible that while annealing at high temperatures, the particles were undergoing further mass transport through dissolving and regrowing. Ostwald ripening may still play a role in hollowing process. The core would leave and incorporate/grow into shell. As a result, a hollow interior space would be eventually generated within the particles. In the end, the particles underwent densification and the hollow structures formed. Note that the hollowing process virtually proceeded simultaneously with the phase conversion in the process of annealing. Therefore, the hollow NiO nanoparticles were obtained. The whole crystallization steps and corresponding morphologic transformations based

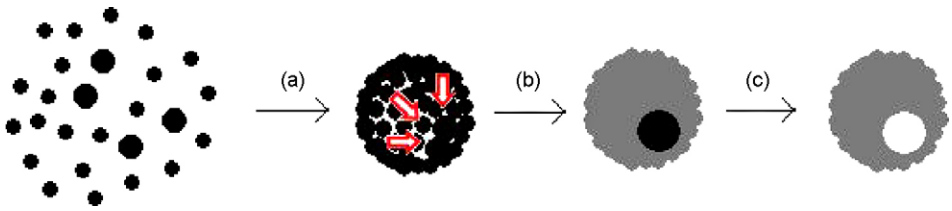

Fig. 5. The schematic diagram of core–shell and hollow particles through Ostwald ripening: (a) aggregating or growing of nanocrystals; (b) formation of core–shell particles and (c) hollowing of particles under annealing. ''Grey and dark regions'' represent the shell and core of core–shell particle, respectively. ''Empty region'' represent hollow hole. ''Arrow line'' is used to represent the mass transfer from small crystals region to larger crystals by Ostwald ripening.

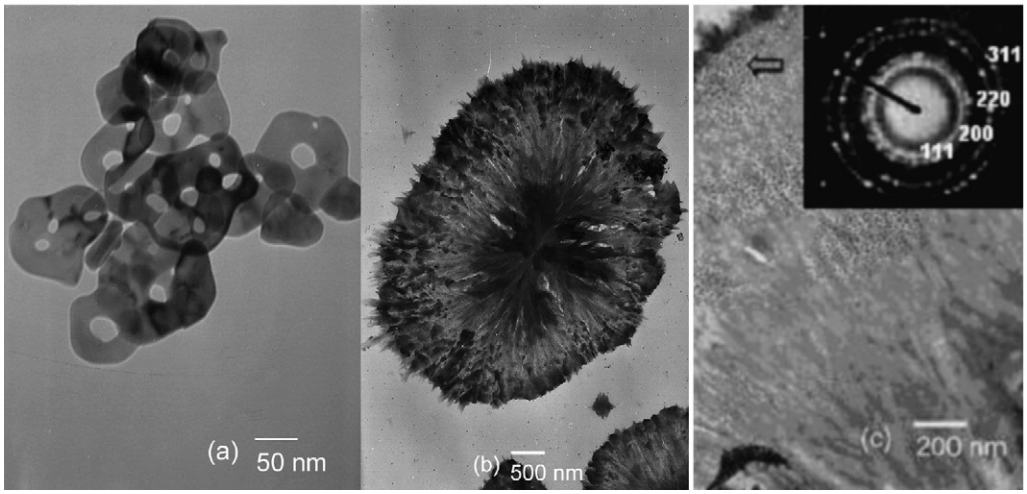

Fig. 6. TEM images and SAED patterns of hollow NiO and Ag/NiO flowers: (a) hollow NiO; (b) Ag/NiO flowers and (c) fringe part of Ag/NiO flower, the insert of SAED patterns.

on Ostwald ripening process have been summarized in schematic diagram, as shown in Fig. 5. The similar process has also been reported by Jia and Gao, when they prepared the Fe_3O_4 core–shell particles [41]. This ''solid-solution-solid'' process has been recently applied to fabrication of various hollow oxide nanostructures [21,27,31,42,43].

Under different hydrothermal temperatures, the obtained samples have different particles structures (core–shell and nanoplates). This can be understood as below. A higher temperature favors to generate a large number of nuclei, which leads to the formation of smaller nanocrystals. However, the small nanocrystals are easy to aggregate together due to the high surface energy. Ostwald ripening process could occur within the aggregate, leading to the formation of core–shell structure. At a lower temperature, a small number of nuclei may generate. The formed nanocrystals are dispersive, and it is not easy to form aggregates. As a result, the nanocrystals grew into the nanoplates.

Further, the hollow NiO particles were impregnated with $AgNO_3$. Interestingly, the Ag/NiO flowers were obtained (Fig. 6b). XRD patterns (Fig. S7 of Supporting information) do not show the diffraction peaks of Ag indicating that the Ag nanocrystals highly dispersed in NiO substrate. The presence of Ag nanocrystals cannot be discerned effectively by XRD, probably due to the small sizes of Ag nanocrystals. Nevertheless, the fringe part of Ag/NiO flower was further characterized by SAED (the insert of Fig. 6c). The SAED patterns exhibit the typical diffraction

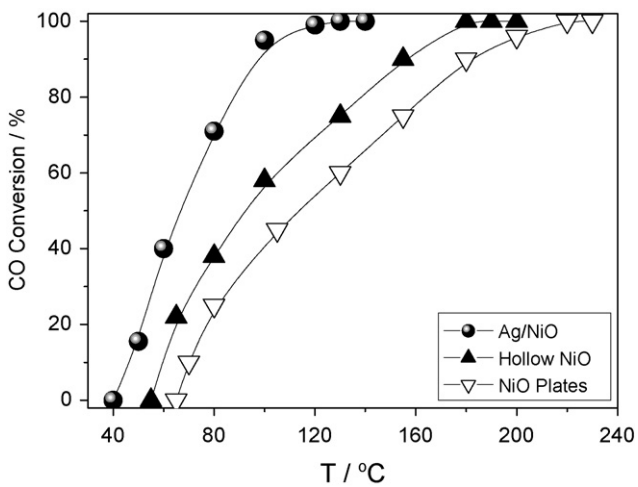

Fig. 7. The oxidation curves for CO over the Ag/NiO and the NiO catalysts with different structures.

rings indexed to (1 1 1), (2 0 0), (2 2 0) and (3 1 1) planes, indicating the fcc symmetry of Ag nanocrystals. The diffraction rings demonstrated the polycrystalline properties of Ag nanocrystals. It could be assumed that a self-assembly process may have occurred. However, the formation mechanism of Ag/NiO flowers is still not clear and needs further research.

3.3. Catalytic activities of the catalysts

Ag/NiO and NiO are important catalyts, and their catalytic activities for CO oxidation were evaluated. As shown in Fig. 7, the complete oxidations of CO over Ag/NiO flowers, hollow NiO nanostructures and NiO nanoplates were achieved at 100, 180 and 220 °C, respectively. The catalytic activity of the hollow NiO catalyst is significantly higher than that of the solid one, which may be closely related to their different BET surface areas and particle structures. The results of N_2 adsorption isotherms show that the surface area (16.6 $m^2\ g^{-1}$) of the hollow NiO hollow sample is higher that that (13.7 $m^2\ g^{-1}$) of the solid counterpart. When the hollow structure was used as a catalyst, a gain of about 100% in surface area is anticipated since the hollow particles possess the outer and inner surfaces. Therefore, the hollow NiO may provide with more active sites for CO oxidation. Moreover, the hollow structure may favor the fluent access to catalyst surface of the reacting gases. The catalytic activity of Ag/NiO catalyst is significantly higher than that of the hollow NiO catalyst, although it has a lower surface area (10.6 $m^2\ g^{-1}$). The higher activity of Ag/NiO catalyst can be ascribed to the presence of Ag, since Ag is an active catalyst for CO oxidation.

4. Conclusions

The novel core–shell $Ni(OH)_2$ and hollow NiO particles can be synthesized by a hydrothermal method. Ostwald ripening process played an important role in the formation of core–shell and hollow nanostructures. Compared with the nanoplates, the hollow NiO catalyst exhibited a higher acitivity for CO oxidation, which was ascribed to its hollow structure. The Ag/NiO flowers showed a high activity due to the high catalytic activity of Ag.

Acknowledgements

This work is supported by Chinese National Science Foundation (Grants 20433010, 20571047) and Chinese Postdoctoral Science Foundation (Grant 20060390057).

Appendix A. Supplementary data

Supplementary data associated with this article can be found, in the online version, at doi:10.1016/j.materresbull.2008.01.009.

References

[1] F. Caruso, R.A. Caruso, H. Möhwald, Science 282 (1998) 1111.
[2] J. Goldberger, R. He, Y. Zhang, S. Lee, H. Yan, H.-J. Choi, P. Yang, Nature 422 (2003) 599.
[3] A.D. Dinsmore, M.F. Hsu, M.G. Nikolaides, M. Marquez, A.R. Bausch, D.A. Weitz, Science 298 (2002) 1006.
[4] Z.Y. Zhong, Y.D. Yin, B. Gates, Y. Xia, Adv. Mater. 12 (2000) 206.
[5] Y. Sun, Y. Xia, Science 298 (2002) 2176.
[6] E. Mathlowitz, J.S. Jacob, Y.S. Jong, G.P. Carino, D.E. Chickering, P. Chaturvedl, C.A. Santos, K. Vijayaraghavan, S. Montgomery, M. Bassett, C. Morrell, Nature 386 (1997) 410.
[7] H. Huang, E.E. Remsen, J. Am. Chem. Soc. 121 (1999) 3805.
[8] C.G. Göltner, Angew. Chem. Int. Ed. 38 (1999) 3155.
[9] K. Kamata, Y. Lu, Y. Xia, J. Am. Chem. Soc. 125 (2003) 2384.
[10] Z. Yang, Z. Niu, Y. Lu, Z. Hu, C.C. Han, Angew. Chem. Int. Ed. 42 (2003) 1943.
[11] S.-W. Kim, M. Kim, W.Y. Lee, T. Hyeon, J. Am. Chem. Soc. 124 (2002) 7642.
[12] J.Y. Kim, S.B. Yoon, J.-S. Yu, Chem. Commun. 11 (2003) 790.
[13] S.P. Naik, A.S.T. Chiang, R.W. Thompson, F.C. Huang, Chem. Mater. 15 (2003) 787.
[14] Y. Hu, J. Chen, W. Chen, X. Lin, X. Li, Adv. Mater. 15 (2003) 726.
[15] Y. Li, J. Shi, Z. Hua, H. Chen, M. Ruan, D. Yan, NanoLetters 3 (2003) 609.

[16] H.G. Yang, H.C. Zeng, Angew. Chem. Int. Ed. 43 (2004) 5206.
[17] C. Wang, K. Tang, Q. Yang, J. Hu, Y. Qian, J. Mater. Chem. 12 (2002) 2426.
[18] Y. Xiong, Y. Xie, Z. Li, C. Wu, R. Zhang, Chem. Commun. 12 (2003) 904.
[19] Y. Matsuzawa, M. Kogiso, M. Matsumoto, T. Shimizu, K. Shimada, M. Itakura, S. Kinugasa, Adv. Mater. 15 (2003) 1417.
[20] Q. Peng, Y. Dong, Y. Li, Angew. Chem. Int. Ed. 42 (2003) 3027.
[21] H.G. Yang, H.C. Zeng, J. Phys. Chem. B 108 (2004) 3492.
[22] Y. Yin, R.M. Rioux, C.K. Erdonmez, S. Hughes, G.A. Somorjai, A.P. Alivisatos, Science 304 (2004) 711.
[23] S. Park, J.-H. Lim, S.-W. Chung, C.A. Mirkin, Science 303 (2004) 348.
[24] B. Liu, H.C. Zeng, J. Am. Chem. Soc. 126 (2004) 8124.
[25] W.Z. Ostwald, Phys. Chem. 22 (1897) 289.
[26] W.Z. Ostwald, Phys. Chem. 34 (1900) 495.
[27] B. Liu, H.C. Zeng, Small 1 (2005) 566.
[28] Z.H. Liang, Y.J. Zhu, X.L. Hu, J. Phys. Chem. B 108 (2004) 3488.
[29] F.S. Cai, G.Y. Zhang, J. Chen, X.L. Gou, H.K. Liu, S.X. Dou, Angew. Chem. Int. Ed. 43 (2004) 4212.
[30] D.B. Wang, C.X. Song, Z.S. Hu, X. Fu, J. Phys. Chem. B 109 (2005) 1125.
[31] Y. Wang, Q. Zhu, H. Zhang, Chem. Commun. 14 (2005) 5231.
[32] B. Sheela, H. Gomathi, G.P. Rao, J. Electroanal. Chem. 394 (1995) 267.
[33] M. Yoshio, Y. Todorov, K. Yamato, H. Noguchi, J. Itoh, M. Okada, T. Mouri, J. Power Sources 74 (1998) 46.
[34] R.C. Makkus, K. Hemmes, J.H.W.D. Wir, J. Electrochem. Soc. 141 (1994) 3429.
[35] D. Zhang, L. Qi, J. Ma, H. Cheng, Adv. Mater. 14 (2002) 1499.
[36] Y. Sun, B. Mayers, Y. Xia, Adv. Mater. 15 (2003) 641.
[37] S. Chah, J.H. Fendler, J. Yi, J. Colloid Interface Sci. 250 (2002) 142.
[38] J.H. Liang, Y.D. Li, Chem. Lett. 32 (2003) 1126.
[39] D.S. Wang, R. Xu, X. Wang, Y.D. Li, Nanotechnology 17 (2006) 979.
[40] S.-L. Che, O. Sakurai, K. Shinozaki, N. Mizutani, J. Aerosol Sci. 29 (1998) 271.
[41] B. Jia, L. Gao, J. Cryst. Growth 303 (2007) 616.
[42] Y. Chang, J.J. Teo, H.C. Zeng, Langmuir 21 (2005) 1074.
[43] H.C. Zeng, J. Mater. Chem. 16 (2006) 649.